

# RESIDUAL STRESS CHARACTERIZATION IN ORTHOTROPIC PLATE BY COMBINING HOLE-DRILLING METHOD AND SPECKLE INTERFEROMETRY

V.S. Pisarev, S.I. Eleonsky, A.V. Chernov

Central Aero-Hydrodynamics Institute named after Prof. N.E. Zhukovsky (TsAGI),  
1, Zhukovsky Street, Zhukovsky Moscow Region, 140180 Russia.

**Keywords:** *keywords list Residual stress; Composite materials; Hole drilling; Electronic speckle-pattern interferometry*

## Abstract

*Novel method for a determination of residual stresses in orthotropic composite plates based on local displacement measurements by electronic speckle-pattern interferometry is developed and verified. The values of hole diameter increments in principal residual stress directions serves as initial experimental deformation. The technique is based on analytical solution of S.G. Lekhnitsky, which describes a stress concentration along the edge of central open hole in rectangular orthotropic plate under one-axis tension in arbitrary direction. A situation when principal directions of residual stresses coincide with principal axes of anisotropy is considered. It is shown that required relations, which connect initial experimental data with residual stress components, are unequivocally solution of the properly posed inverse problem. An availability of interference fringe patterns, a quality of which is high enough for reliable recognising of fringe orders at the hole edge immediately, is the essential experimental foundation of the approach developed.*

## 1 Introduction

Laminated fibre-reinforced composites currently used in airplane structures are often subjected to residual stresses due to manufacturing process [1-2]. Since residual stresses influence the properties of the composite structures

significantly, they have to be taken into account in both design and numerical modelling [3-6]. Thus the study and the knowledge of mechanical behaviour and strength of composite structures essentially imply the accurate determination of the residual stress state. Traditional strain gauge version of the hole drilling method is widely used experimental technique for residual stress characterization in orthotropic materials [7-9]. But a reliability of this approach is sometimes limited by point-wise character of strain measurements near drilled hole.

To improve a situation full-field optical interferometric techniques have been involved. In such cases multiple-point over-deterministic approach is used to solve the residual stress problem. The approach, which is based on the nonlinear least square error minimization between the experimental data obtained by moiré method and their numerical representation, has been developed [10-12]. Proposed solution algorithm is of unnecessarily complex from a numerical point of view since it was developed in the grating interferometry. An acquisition of initial experimental data by electronic speckle-pattern interferometry is the way of some simplifying residual stress determination by various least square algorithms [13-14]. In general case both above-mentioned procedures employ complex finite element modelling to receive calibration coefficients out of the hole boundary and further inverse problem solution. The point is that the

theoretical solution of stress/strain concentration problem for through circular hole in orthotropic plate under one-axis tension by any angle with respect to principal anisotropy directions exists at the hole edge only [15]. Unfortunately, the excellent theoretical considerations provided with artificial interference images presented in works [10-14] do not strengthened by reliable experimental verification.

The paper concerns a determination of residual stresses in composite plate by drilling through hole and further measurements of hole diameter increments in principal stress directions by electronic speckle-pattern interferometry. Such an approach has been previously developed and comprehensively verified for metallic thin plates [16-18]. The technique proposed is based on analytical solution of S.G. Lekhnitsky [15]. A situation when principal directions of residual stresses coincide with principal axes of anisotropy is considered. Required relations, which connect initial experimental data with residual stress components, represent by itself unequivocally solution of the properly posed inverse problem. An availability of interference fringe patterns, a quality of which is high enough for reliable recognising of fringe orders at the hole edge immediately, is the experimental foundation of the approach developed. The accuracy analysis of the method performed by two different ways is presented.

## 2 Formulation of the problem

Residual stress field in orthotropic plate is below considered as uniform both in the normal to the surface direction and in tangential directions over the probe hole diameter. This means that two unknown parameters  $\sigma_1$  and  $\sigma_2$  have to be determined for complete characterization of residual stress values at each point of interest. These parameters can be presented as a vector  $\mathbf{s}$ :

$$\mathbf{s} = \{\sigma_1, \sigma_2\}^T. \quad (1)$$

Initially measured parameters used for residual stress deriving can be also arranged as a vector  $\mathbf{d}$ . The relation between unknown vector  $\mathbf{s}$  and vector  $\mathbf{d}$  is expressed as:

$$\mathbf{A} \cdot \mathbf{s} = \mathbf{d}, \quad (2)$$

where matrix  $\mathbf{A}$  defines in explicit form so-called transition model [16,17]. Such a model is a set of relations derived from mechanical formulation of the problem involved, which has also to include the material mechanical properties and the probe hole geometry. Equation (2) shows that required vector  $\mathbf{s}$  can be obtained by means of inverse problem solution [19]:

$$\mathbf{s} = \mathbf{A}^{-1} \cdot \mathbf{d}. \quad (3)$$

Minimal possible dimension of matrix  $\mathbf{A}$  from equations (2) and (3) is  $[n \times n] = [2 \times 2]$  because a length of vector  $\mathbf{s}$  (1) is equal to  $n=2$ . If matrix  $\mathbf{A}$  is a regular positively defined square  $[n \times n]$  matrix, the inverse problem is properly posed and the unequivocally solution of equation (3) exists [19]. To obtain matrix  $\mathbf{A}$  in an explicit form we must define a form of the vector  $\mathbf{d}$  by unique way.

It is quite evident that properly posed square matrix  $\mathbf{A}$  can be only constructed if a vector  $\mathbf{d}$  is formed proceeding from experimental data related to principal stress direction. Vector  $\mathbf{d}$  should consist of experimental parameters, which can be reliably measured within the highest possible accuracy. Hole diameter increments  $\Delta u$  and  $\Delta v$  in principal strain direction  $\varepsilon_1$  and  $\varepsilon_2$ , respectively, are precisely the parameters, which certainly fit into the above-mentioned condition [17]. An availability of two increments  $\Delta u$  and  $\Delta v$  referred to contour of through hole drilled in orthotropic plate allows us to form a vector  $\mathbf{d}$  of required dimension  $n=2$ :

$$\mathbf{d} = \{\Delta u, \Delta v\}^T. \quad (4)$$

Both components of vector  $\mathbf{d}$  (4) can be obtained by electronic speckle-pattern interferometry as it will be shown below.

## 3 Main relations for residual stresses determination

The basic assumption, which is mainly used for deriving residual stress values on a base of the hole drilling method, consists of the fact that a

small hole is made in 2D stress field, which is uniform independently of each from two principal stress directions on the object surface. This means that a possible influence of stress gradients at the hole proximity is not taken into account. The superposition principal for local displacement and strain fields corresponding to each in-plane strain tensor component is also postulated. A through hole of diameter  $2r_0$  is made at some point of the surface area under consideration. The centre of this hole is a conventional point where the residual stresses must be determined.

A distribution of circumferential strain component  $\varepsilon'_\theta$  along the edge of small circular hole, when the plane stress conditions are valid in thin plate, can be expressed in the general form as [15]:

$$\varepsilon'_\theta = \Phi(\theta, \varphi) \quad (5)$$

where  $\theta$  is the polar angle in the co-ordinate system referred to the hole centre that is counted anti-clock wise from  $x$ -axis;  $\varphi$  is the angle between principal anisotropy direction  $E_1$  and a direction of the tension by nominal stress  $\sigma_0$  (see Figure 1). Accordingly to the developed approach required values of principal residual strain components are derived from relation (5) by the following way [16, 17]:

$$\varepsilon'_1 = \Phi(\theta = \theta_0, \varphi), \quad \varepsilon'_2 = \Phi(\theta = \theta_0 - \pi/2, \varphi) \quad (6)$$

where the angle  $\theta_0$  defines a point in the hole edge where maximal value of principal strain is reached.

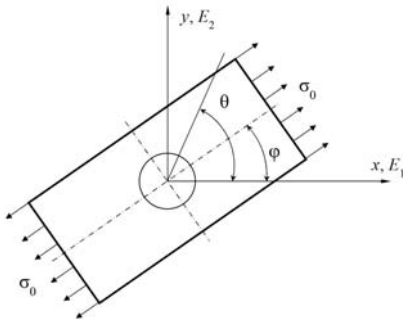


Fig. 1. Notations used for a determination of stress concentration coefficients along the probe hole edge.

Foundations of the hole drilling method give the following relations between in-plane principal strain components [17]:

$$\varepsilon'_1 - \varepsilon''_1 = \varepsilon_1^{III}, \quad \varepsilon'_2 - \varepsilon''_2 = \varepsilon_2^{III}, \quad (7)$$

where  $\varepsilon_1$  and  $\varepsilon_2$  are principal residual strains. Roman superscripts denote mechanical state of the object surface. State I represents a two-axes loading of the element of the material volume containing the probe hole. State II is an initial deformed state of the object surface area of interest caused by two-dimensional field of residual stress before drilling a hole. The components of this stress field are the principal residual stresses  $\sigma_1''$  and  $\sigma_2''$  to be determined. State III is related to residual stress energy release after hole drilling and can be represented as a difference between State I and State II. Corresponding parameters of State III have to be derived from interference fringe patterns and those of States I and II should be described analytically or numerically in a general form proceeding from the elasticity theory relations.

Principal strains  $\varepsilon_1'$  and  $\varepsilon_2'$  related to State I can be always expressed by using the solution of elastic strain/stress concentration problem for open circular hole in thin both isotropic and anisotropic plate. Developed approach is based on Lekhnitsky's solution, which describes local stress distribution along the edge of through circular hole in rectangular orthotropic plate under one-axis tension [15]. This solution is valid for different orientation of the tension direction with respect to principal anisotropy axes. The notation involved is shown in Figure 1. Here and below Cartesian co-ordinate system  $(x, y)$  defines principal anisotropy axes with  $x$ -axis coincides with the direction of the greater elasticity modulus  $E_1$ . Polar angle  $\theta$  is one of the arguments of stress concentration function and indicates position of the point of interest at the hole boundary. This angle is always counted in anti-clock wise direction from the point of intersection of the hole edge with  $x$ -axis as it is shown in Figure 1. The angle  $\varphi$  between  $E_1$ -direction and a direction of tensile stress  $\sigma_0$  is the second argument of stress concentration function along the hole edge. For thin orthotropic plate with central open hole subjected to one-axis tension by nominal stress  $\sigma_0$ , which is applied sufficiently far from the hole, the local stress distributions is expressed as:

$$\sigma_{\theta} = \sigma_0 f(\varphi, \theta) \quad (8)$$

where  $f(\varphi, \theta)$  is the stress concentration function. The function (8) has the following form [15]:

$$f(\varphi, \theta) = \frac{E_{\theta}}{E_1} \left\{ \begin{aligned} & -k[\cos^2 \varphi - (k+n)\sin^2 \varphi]\cos^2 \theta + \\ & [(1+n)\cos^2 \varphi - k\sin^2 \varphi]\sin^2 \theta - \\ & -n(k+n)\sin \varphi \cos \varphi \sin \theta \cos \theta \end{aligned} \right\} \quad (9)$$

where tangential elastic modulus  $E_{\theta}$  is defined as:

$$\frac{1}{E_{\theta}} = \frac{\sin^4 \theta}{E_1} + \frac{2\sin^2 \theta \cos^2 \theta}{E_1} + \frac{\cos^4 \theta}{E_2} \quad (10)$$

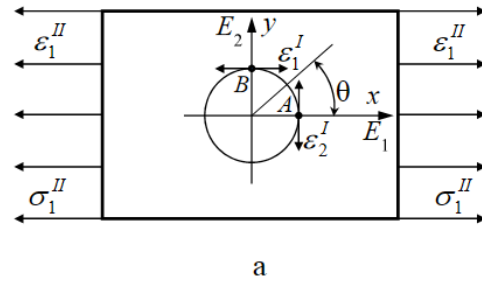
where  $E_2$  is the lesser principal elasticity modulus in the direction of  $y$ -axis. Other parameters from formula (9) are:

$$k = \sqrt{\frac{E_1}{E_2}}, \quad n = \sqrt{2(k+1)} \quad (11)$$

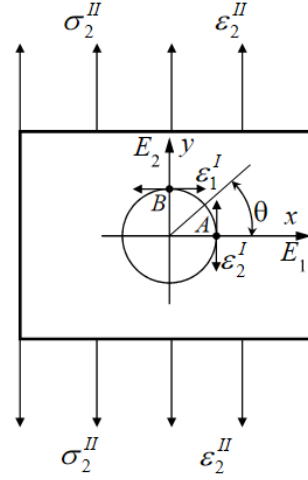
Below for deriving required relations the following well-known formula is used:

$$\frac{V_{12}}{E_1} = \frac{V_{21}}{E_2} \quad (12)$$

In order to obtain the explicit form of strain concentration coefficients (6) the angle  $\varphi$  value has to be prescribed. This paper only concerns of the case when principal residual stress (strain) directions coincide with principal anisotropy axes ( $x$ ,  $y$ ). Thus to solve the problem of determination of two residual stress components two cases of applying external load have to be considered, namely  $\varphi=0$  and  $\varphi=\pi/2$ . In this case a value of the angle  $\theta$  from relation (6) is equal to  $\theta_0 = \pi/2$ . Rectangular orthotropic plate with central circular hole under one-axis tension in  $E_1$ -direction and  $E_2$ -direction is shown in Figure 2a and 2b, respectively. Applied nominal stresses  $\sigma_1^H$  and  $\sigma_2^H$  are principal residual stress components to be experimentally determined.



a



b

Fig. 2. A scheme for determination of strain concentration coefficients for plate with circular hole under one-axis tension along principal anisotropy direction  $E_1$  (a) and  $E_2$  (b).

A determination of residual stresses proceeding from in-plane displacement component measurements for points belonging to small hole edge implies the deformation representation of the hole drilling method (7). That is why a formulation of required linear algebraic equation system needs using the strain concentration function. This function denoted as  $F(\theta)$  is defined by relation (8):

$$\varepsilon_{\theta} = \frac{\sigma_{\theta}}{E_{\theta}} = \sigma_1^H F(\varphi, \theta) \quad (13)$$

where  $F(\varphi, \theta) = f(\varphi, \theta)/E_{\theta}$ , and  $E_{\theta}$  follows from relation (10). For the case  $\varphi=0$  keeping in mind formula (9) relation (13) takes the following form:

$$\varepsilon_{\theta} = \frac{\sigma_1^H}{E_1} [-k \cos^2 \theta + (1+n)\sin^2 \theta] = \varepsilon_1^H F_1(\theta) \quad (14)$$

For the case  $\varphi=\pi/2$  taking into account formula (9) relation (13) gives:

$$\begin{aligned}\varepsilon_{\theta} &= \frac{\sigma_2''}{E_1} \left[ k(k+n) \cos^2 \theta - k \sin^2 \theta \right] = \\ &= \frac{\sigma_2''}{E_2} \left[ \left(1 + \frac{n}{k}\right) \cos^2 \theta - \frac{1}{k} \sin^2 \theta \right] = \varepsilon_2'' F_2(\theta)\end{aligned}\quad (15)$$

Relations (14) and (15) in view of the superposition principal and formula (10) allow us a determination of strain concentration coefficients at point A ( $\theta=0$ ) and at point B ( $\theta=\pi/2$ ), which are essential for constructing the relations of type (7):

$$\begin{aligned}\varepsilon_1^I &= \frac{1}{E_1} \left\{ (1+n)\sigma_1'' - k\sigma_2'' \right\} \\ \varepsilon_2^I &= \frac{1}{E_2} \left\{ \left(1 + \frac{n}{k}\right)\sigma_2'' - \frac{1}{k}\sigma_1'' \right\}\end{aligned}\quad (16)$$

To complete the left-hand side of the basic equation of the hole-drilling method (7) we have to express initial strains at points A and B before the hole drilling. These strains follow from orthotropic Hook's law for plane stress conditions with using relation (12):

$$\varepsilon_1'' = \frac{\sigma_1''}{E_1} - \frac{\nu_{12}\sigma_2''}{E_1}, \quad \varepsilon_2'' = \frac{\sigma_2''}{E_2} - \frac{\nu_{21}\sigma_1''}{E_2}\quad (17)$$

Relations (16) and (17) form the left-hand side of equation system (7), which is essential for a determination of residual stress components in orthotropic plate when a through hole is drilled.

A formulation of the right-hand side of linear algebraic equation system (7) is based on some quite evident considerations, which follow from a type of strain concentration function (14) and (15). Firstly, for State I distributions of in-plane displacement components  $u$  and  $v$  along small hole edge of  $r_0$  radius taking into account relations (16) can be presented in the following form:

$$\begin{aligned}u^I(\theta) &= \frac{r_0}{E_1} \left\{ (1+n)\sigma_1'' - k\sigma_2'' \right\} \cos \theta = \frac{r_0}{E_1} A^I \cos \theta \\ v^I(\theta) &= \frac{r_0}{E_2} \left\{ \left(1 + \frac{n}{k}\right)\sigma_2'' - \frac{1}{k}\sigma_1'' \right\} \sin \theta = \frac{r_0}{E_2} B^I \sin \theta\end{aligned}\quad (18)$$

Relations (18) allow us to obtain a distribution of circumferential strain  $\varepsilon_{\theta}^I$  along the boundary of central open hole of  $r_0$  radius in thin plate [16]:

$$\begin{aligned}\varepsilon_{\theta}^I &= \frac{1}{r_0} \left\{ \frac{\partial v^I(\theta)}{\partial \theta} \cos \theta - \frac{\partial u^I(\theta)}{\partial \theta} \sin \theta \right\} = \\ &= \frac{A^I}{E_1} \cos^2 \theta - \frac{B^I}{E_2} \sin^2 \theta\end{aligned}\quad (19)$$

A combination of relations (18) and (19) for  $\theta=0$  and  $\theta=\pi/2$  allows us to establish that:

$$\varepsilon_1^I = \frac{\Delta u^I}{2r_0}, \quad \varepsilon_2^I = \frac{\Delta v^I}{2r_0}\quad (20)$$

where  $\Delta u^I = 2u^I(\theta=0)$  and  $\Delta v^I = 2v^I(\theta=\pi/2)$  are the increments of real hole of  $2r_0$  diameter caused by two-axes plate loading in principal anisotropy directions  $E_1$  and  $E_2$ , respectively.

Analogous way with using relations (17) gives the following relations:

$$\varepsilon_1'' = \frac{\Delta u''}{2r_0}, \quad \varepsilon_2'' = \frac{\Delta v''}{2r_0}\quad (21)$$

where  $\Delta u'' = 2u''(\theta=0)$  and  $\Delta v'' = 2v''(\theta=\pi/2)$  are the increments of conventional hole of  $2r_0$  diameter caused by two-axes plate loading in principal anisotropy directions  $E_1$  and  $E_2$ , respectively.

A difference in relations (20) and (21) gives the right-hand side of equation system (7):

$$\begin{aligned}\varepsilon_1^I - \varepsilon_1'' &= \frac{1}{2r_0} (\Delta u^I - \Delta u'') = \frac{\Delta u'''}{2r_0} = \frac{\Delta u}{2r_0} \\ \varepsilon_2^I - \varepsilon_2'' &= \frac{1}{2r_0} (\Delta v^I - \Delta v'') = \frac{\Delta v'''}{2r_0} = \frac{\Delta v}{2r_0}\end{aligned}\quad (22)$$

where  $\Delta u$  and  $\Delta v$  are the diameter increments of real hole of  $2r_0$  diameter drilled in 2D residual stress field in principal anisotropy directions  $E_1$  and  $E_2$ , respectively. Required values of hole diameter increments  $\Delta u$  and  $\Delta v$  are experimentally measured by electronic speckle-pattern interferometry. A substitution of relations (14) and (15) into relations (22) defines the explicit form of equation system (7) in the case when principal directions of residual stresses (strains) coincide with principal anisotropy directions of orthotropic plate:

$$\begin{aligned}\frac{1}{E_1} \left\{ (1+n)\sigma_1'' - k\sigma_2'' \right\} - \frac{1}{E_1} \left\{ \sigma_1'' - \nu_{12}\sigma_2'' \right\} &= \frac{\Delta u}{2r_0} \\ \frac{1}{E_2} \left\{ \left(1 + \frac{n}{k}\right)\sigma_2'' - \frac{1}{k}\sigma_1'' \right\} - \frac{1}{E_2} \left\{ \sigma_2'' - \nu_{21}\sigma_1'' \right\} &= \frac{\Delta v}{2r_0}\end{aligned}\quad (23)$$

Relations (23) correspond to equation (2) with vector  $\mathbf{d}$  of form (4). Matrix  $\mathbf{A}$  in this case is:

$$A = 2r_0 \begin{bmatrix} \frac{n}{E_1} & \frac{(v_{12} - k)}{E_1} \\ \frac{(v_{21} - \frac{1}{k})}{E_2} & \frac{n}{kE_2} \end{bmatrix} \quad (24)$$

Required solution of equation (3) based on matrix  $\mathbf{A}$  (24) that defines both residual stress components of interest has the following form:

$$\sigma_1'' \equiv \sigma_1 = \frac{E_1}{2r_0 k} \left\{ \frac{n\Delta u + \left(1 - \frac{v_{12}}{k}\right)\Delta v}{\frac{n^2}{k} - (k - v_{12})\left(\frac{1}{k} - v_{21}\right)} \right\} \quad (25)$$

$$\sigma_2'' \equiv \sigma_2 = \frac{E_2}{2r_0} \left\{ \frac{n\Delta v + k^2\left(\frac{1}{k} - v_{21}\right)\Delta u}{\frac{n^2}{k} - (k - v_{12})\left(\frac{1}{k} - v_{21}\right)} \right\}$$

Residual stress component values (25) represent by itself the unequivocally solution of the properly posed inverse problem (3) with vector  $\mathbf{d}$  of form (4). For isotropic case, when  $E_1=E_2=E$ ,  $v_{12}=v_{21}=v$ ,  $k=1$  and  $n=2$ , relations (25) coincide with formulae obtained in works [16, 17]. An explicit form of matrix  $\mathbf{A}^{-1}$  follows from relations (25):

$$A^{-1} = \frac{1}{2r_0 \left\{ \frac{n^2}{k} - (k - v_{12})\left(\frac{1}{k} - v_{21}\right) \right\}} \times \begin{bmatrix} \frac{E_1 n}{k} & \frac{E_1 \left(1 - \frac{v_{12}}{k}\right)}{k} \\ E_2 k^2 \left(1 - \frac{v_{21}}{k}\right) & E_2 n \end{bmatrix} \quad (26)$$

#### 4 Measurement procedure

Electronic speckle-pattern interferometry (ESPI) serves for experimental determination of in-plane displacement components [18,20]. Well-known optical system with normal illumination with respect to plane object surface and two symmetrical observation directions is employed (Figure 3). Two images of the surface area of interest, which correspond to initial and final mechanical state of the object, are consequently recorded by CCD camera Videoscans USB-285

(1200x800 pixels) and stored as digital files. A visualization of interference fringe patterns is performed by digital subtraction of two above-mentioned images.

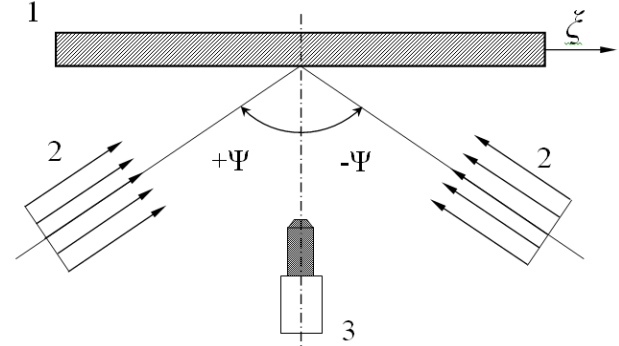


Fig. 3. General scheme of obtaining interference fringe patterns for deriving in-plane displacement components by ESPI; 1 – Investigated object; 2 – Illuminating plane waves of laser light; 3 – CCD camera.

When a projection of illumination directions onto plane surface of the investigated object coincides with  $\xi$ -direction, interference fringe pattern is described as:

$$d_\xi = N \frac{\lambda}{2 \sin \Psi} \quad (27)$$

where  $d_\xi$  is in-plane displacement component in  $\xi$ -direction;  $N = \pm 1; \pm 2; \pm 3, \dots$  are the absolute fringe orders;  $\lambda$  is the wavelength of laser illumination;  $\Psi = \pi/4$  is the angle between inclined illumination and normal observation directions. When  $\xi$ -direction coincides with  $x$ -axis and  $y$ -axis displacement component  $u$  and  $v$  can be derived accordingly to formula (27), respectively. Simultaneous determination of both in-plane displacement components  $u$  and  $v$  is reached by combining of two optical system of type shown in Figure 3 into united device. An identification of real physical sign of each in-plane displacement component with respect to co-ordinates axes  $x$  and  $y$  shown in Figure 1 is reached by recording interferograms with additional phase shift, a sign and value of which are known before the experiment [18]. Compact diode laser with wavelength  $\lambda = 532$  nm is used as a source of the coherent illumination. The real view of the interferometer is shown in Figure 4.

Practically plane illuminating wave, which comes from the right-hand side of Figure 4, is divided by front into two approximately equal

parts. The upper part of illuminating light and two mirrors denoted by number 1 forms the interferometer branch for  $v$ -component determination. The lower part of illuminating wave and three mirrors denoted by number 2 forms the interferometer branch for  $u$ -component determination. The measurement area 3 is of dimensions  $40 \times 40 \text{ mm}^2$ . Required images pairs are recorded by CCD camera Videoscan USB-285 equipped with the lens AF-S VR Micro-Nikkor 105 mm f/2.8G IF-ED denoted by number 4. The specimen 6 is mounted on the upper part of traditional kinematically designed mount [21]. This mount denoted by number 5 in Figure 4 allows us to perform hole drilling out of the interferometer system after the first exposure and further precise returning back the drilled specimen and recording the final surface state. Some of drilled holes are denoted by number 7. The measurement ESPI system shown in Figure 4 is capable of fast and reliable obtaining interference fringe patterns caused by through hole drilling in orthotropic plate.

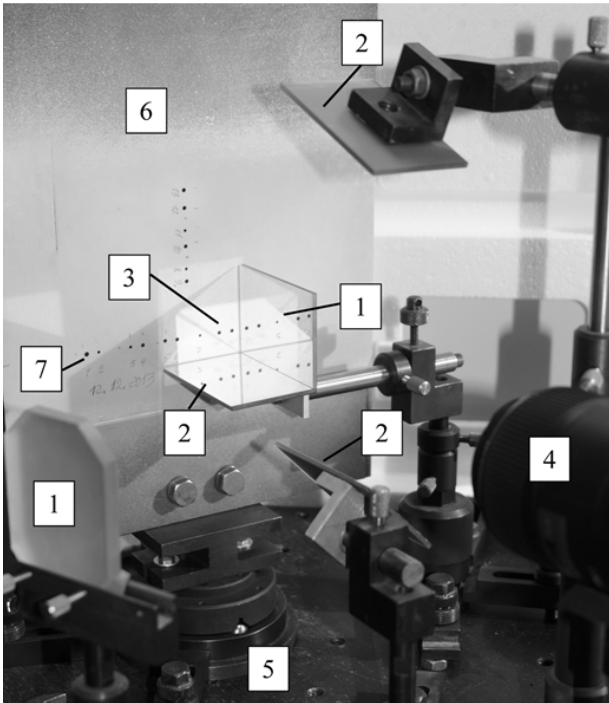


Fig. 4. Real view of the interferometer system.

## 5 Residual stress determination

### 5.1 Rectangular composite plate

The first object of experimental investigations represents by itself rectangular orthotropic plate of dimensions  $400 \times 200 \times 6 \text{ mm}^3$  made from layered fibre-reinforced material (see Figure 4). Generalized mechanical properties and anisotropy parameters of the plate denoted as specimen 1 are:

$$\begin{aligned} E_1 &= 69.2 \text{ GPa}, E_2 = 30.5 \text{ GPa}, \\ G_{12} &= 21.9 \text{ GPa}, \nu_{12} = 0.58, \nu_{21} = 0.25, \\ k &= 1.50, n = 2.24. \end{aligned} \quad (28)$$

A set of nine probe holes is performed along the line that coincides with  $E_2$ -direction and is located by 150 mm distance from the specimen edge. A distance between centres of neighbouring holes is more than 15 mm. Diameters of drilled holes are presented in Table 1. Interferometer optical system shown in Figures 3 and 4 is used for a determination of both in-plane displacement components.

Interference fringe patterns obtained for point 4 are shown in Figure 5. Horizontal symmetry axis in Figure 5a and vertical symmetry axis in Figure 5b coincides with principal anisotropy direction  $E_1$  and  $E_2$ , respectively. High quality of these interferograms should be specially noted. The same quality is inherent in all interferometric images recorded for other drilled holes. Superimposed interference fringe patterns, which correspond to the images shown in Figure 5 but recorded with additional phase shift, are presented in Figure 6. These interferograms reveal that hole diameter is increased in both  $x$ -direction ( $u$ -displacement component, elasticity modulus  $E_1$ ) and  $y$ -direction ( $v$ -displacement component, elasticity modulus  $E_2$ ). Physical sign identification is performed accordingly to the procedure used in work [18].

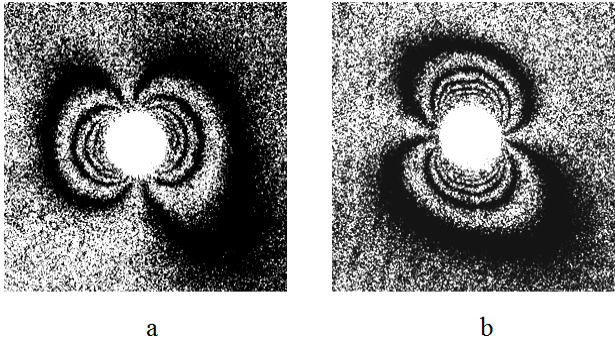


Fig. 5. Specimen 1. Interference fringe patterns obtained for point 4 in terms of in-plane displacement component  $u$  (a) and  $v$  (b).

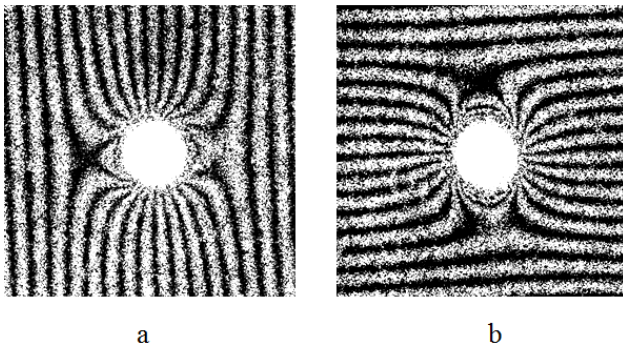


Fig. 6. Specimen 1. Interference fringe patterns obtained for point 4 in terms of in-plane displacement component  $u$  (a) and  $v$  (b) with additional phase shift.

Table 1. The results of interference fringe patterns interpretation and residual stress determination for specimen 1.

Point number	Hole diameter $2r_0$ , mm	Fringe order interferences		Hole diameter increments		Residual stress values	
		$\Delta N_u$ , fringes	$\Delta N_v$ , fringes	$\Delta u$ , $\mu\text{m}$	$\Delta v$ , $\mu\text{m}$	$\sigma_1$ , MPa	$\sigma_2$ , MPa
3	2.0	8.0	10.5	3.04	4.18	73.5	61.9
2	2.0	7.0	10.0	2.66	3.8	65.9	57.8
7	2.0	7.5	9.5	2.85	3.61	68.3	56.5
8	2.0	9.0	10.0	3.42	3.8	79.4	61.5
11	2.0	8.0	9.5	3.04	3.61	71.7	57.4
4	2.5	10.0	13.0	3.8	4.94	73.4	61.4
5	2.5	10.0	13.0	3.8	4.94	73.4	61.4
9	2.5	11.0	13.5	4.18	5.13	79.5	64.7
10	2.5	11.5	13.0	4.37	4.94	81.5	63.7

The results of interference fringe patterns interpretation in terms of fringe order differences and hole diameter increments in principal stress directions are listed in Table 1. Values of  $\Delta N_u$  and  $\Delta N_v$  are determined by direct counting fringe orders between two basic points. These points are the points of intersection of horizontal symmetry axis and vertical symmetry axis related to the hole centre in the case of  $\Delta N_u$ -counting (Figure 5a) and  $\Delta N_v$ -counting (Figure 5b), respectively. The values  $\Delta N_u$  and

$\Delta u$  as well as  $\Delta N_v$  and  $\Delta v$  are connected by formula (27) for  $\lambda = 532$  nm. All interferograms recorded evidence that principal directions of residual stresses coincide with principal axes of anisotropy. This means that residual stress values can be reliably calculated by using relations (25). To do this experimental information from Table 1 and parameters (28) are involved. Data presented in Table 1 show that residual stress component values obtained for different hole diameters are in a good agreement. At first this fact confirms a reliability of the technique developed. Second, we can say with a confidence that real plane stress state in orthotropic plate under study is of pure membrane character. The last circumstance is of great importance when the accuracy of residual stress determination is estimated by constructing reference fringe patterns. Remarkable capabilities of this approach in the course of residual stress determination in metallic materials have been demonstrated in works [16-18].

### 5.2 Square composite plate

Square composite plate of dimensions  $150 \times 150 \times 6$  mm<sup>3</sup> made from layered fibre-reinforced material serves as the second object of experimental investigations (specimen 2). Generalized mechanical properties and anisotropy parameters of the plate are:

$$\begin{aligned} E_1 &= 73.9 \text{ GPa}, E_2 = 29.5 \text{ GPa}, \\ G_{12} &= 19.7 \text{ GPa}, \nu_{12} = 0.58, \nu_{21} = 0.23, \\ k &= 1.58, n = 2.27 \end{aligned} \quad (29)$$

A set of seven probe holes is performed along the line that coincides with  $E_2$ -direction and is located by 50 mm distance from the specimen edge. A distance between centres of neighbouring holes is more than 15 mm. Table 2 includes diameters of drilled holes, for points where the most reliable results are obtained.

Interference fringe patterns visualised for point 2 and 5 are shown in Figure 7 and 8, respectively. Horizontal symmetry axis in Figures 7a, 8a and vertical symmetry axis in Figures 7b, 8b coincide with principal anisotropy direction  $E_1$  and  $E_2$ , respectively. High quality of these interferograms should be specially noted. The same quality is inherent in

all interferometric images recorded for other drilled holes. Superimposed interference fringe patterns, which correspond to the images shown in Figure 7 and 8 but recorded with additional phase shift, show that hole diameter is increased in both  $x$ -direction ( $u$ -displacement component, elasticity modulus  $E_1$ ) and  $y$ -direction ( $v$ -displacement component, elasticity modulus  $E_2$ ).

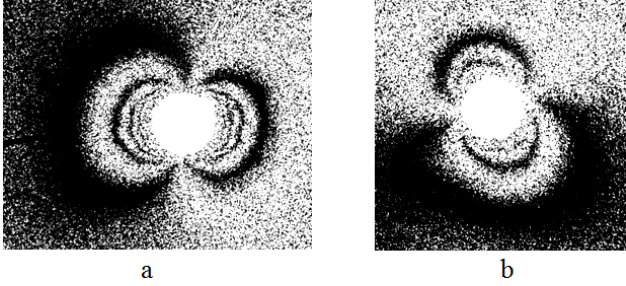


Fig. 7. Specimen 2. Interference fringe patterns obtained for point 2 in terms of in-plane displacement component  $u$  (a) and  $v$  (b).

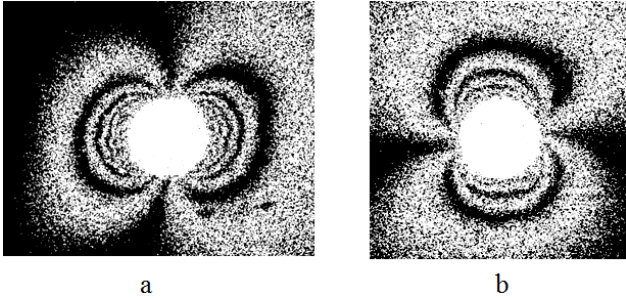


Fig. 8. Specimen 2. Interference fringe patterns obtained for point 5 in terms of in-plane displacement component  $u$  (a) and  $v$  (b).

*Table 2.* The results of interference fringe patterns interpretation and residual stress determination for specimen 2.

Point number	Hole diameter $2r_0$ , mm	Fringe order interferences		Hole diameter increments		Residual stress values	
		$\Delta N_u$ , fringes	$\Delta N_v$ , fringes	$\Delta u$ , $\mu\text{m}$	$\Delta v$ , $\mu\text{m}$	$\sigma_1$ , MPa	$\sigma_2$ , MPa
2	2.0	9.5	6.0	3.61	2.28	81.0	46.0
5	2.5	12.0	7.5	4.56	2.85	81.0	46.0
6	3.2	15.0	11.0	5.70	4.18	81.0	50.0

All obtained interferograms evidence that principal directions of residual stresses coincide with principal axes of anisotropy. This means that residual stress values can be reliably calculated by using relations (25). To do this experimental information from Table 2 and parameters (29) are involved. Data presented in Table 2 show that residual stress component

values obtained for different hole diameters are in a good agreement. At first, this fact again confirms a reliability of the technique developed. Second, real plane stress state in orthotropic composite plate under study corresponds to the pure membrane conditions.

## 5 Metrological verification

### 5.1 Mathematically based accuracy analysis

An availability of direct matrix  $\mathbf{A}$  (24) from equation (2) and inverse matrix  $\mathbf{A}^{-1}$  (26) from equation (3) in their explicit forms allows us quantitative estimations of errors inherent in a determination of residual stress components accordingly to the approach developed in works [17, 22]. In such a case the upper bound of the error made in calculating each component of unknown vector  $\mathbf{s}$  can be estimated in the following form:

$$\frac{|\delta s_i|}{\|s\|} \leq \frac{\text{cond}A}{\sqrt{2}} \frac{\|\delta d\|}{\|d\|} \quad (30)$$

where  $i=1,2$ ;  $|\delta s_i|$  is an error made in the determination of  $s_i$ -component;  $\text{cond}A$  is the condition number of matrix  $\mathbf{A}$ . The symbol  $\|\cdot\|$  denotes vector and matrix norm. The condition number is defined as:

$$\text{cond}A = \|\mathbf{A}\| \cdot \|\mathbf{A}^{-1}\|. \quad (31)$$

Vector norms included in inequality (30) are defined as a length of corresponding vector ( $\|s\| = \sqrt{s_1^2 + s_2^2}$  and so on). Matrix norm from relations (30) and (31), which corresponds to this vector norm, is Euclid norm [23]:

$$\|\mathbf{A}\| = \left\{ \sum_{i,j} |a_{ij}|^2 \right\}^{1/2} \quad (32)$$

where  $a_{ij}$  are the elements of arbitrary matrix  $\mathbf{A}$ .

Further analysis needs involving a set of real experimentally obtained data. Let us consider now typical error estimation, which follows from inequality (30) for the hole related to point 4 from Table 1. First, the condition number has to be calculated. A substitution of parameters (28) into relations (24) and (26) taking into account definition (32) and further

insertion of both obtained results into definition (31) give:

$$condA = 0.6 \cdot 4.92 = 2.95 \quad (33)$$

Next step resides in an estimation of the error inherent in a determination of hole diameter increments  $\Delta u$  and  $\Delta v$ . Required estimation directly follows from formula (27):

$$|\delta(\Delta u)| = |\delta(\Delta v)| = \frac{\lambda \delta N}{2 \sin \Psi} \quad (34)$$

where  $\lambda=0.532 \mu\text{m}$  is the wavelength;  $\delta N$  is an error in counting the absolute fringe orders;  $\Psi = \pi/4$  is the sensitivity angle. An accuracy in the determination of absolute fringe orders  $\delta N=0.5$  fringe can be reliably achieved as a difference between dark and bright neighbouring fringes. Thus inequality (34) gives:

$$|\delta(\Delta u)| = |\delta(\Delta v)| \leq 0.2 \cdot 10^{-3} \text{mm} \quad (35)$$

The following parameters, which are based on inequalities (35), definition (32) and data of Table 1, are also needed in the course of required accuracy analysis:

$$\begin{aligned} \|d\| &= 6.23 \cdot 10^{-3} \text{mm}, \\ \|\delta d\| &= 0.28 \cdot 10^{-3} \text{mm}, \\ \|s\| &= 95.7 \text{MPa}. \end{aligned} \quad (36)$$

Substituting the values of parameters (33) and (36) into estimation (30) gives:

$$|\delta s_i| \leq 9.0 \text{MPa} \quad (37)$$

Inequality (37) conservatively describes the upper limit of the error made in the determination of each residual stress component. This fact follows from a definition of the adopted Euclid matrix norm (32) as it is shown in work [24]. The main sources of estimated error are a structure of matrix  $\mathbf{A}$  (24) and errors made in a determination of in-plane displacement components accordingly to formulae (35). It should be also noted that estimations (37) is obtained for maximal possible error in fringe order counting  $\delta N=0.5$  fringe. Relative errors in a determination of residual stress components for the case considered are:

$$\frac{|\delta \sigma_1|}{\sigma_1} \leq 0.12, \quad \frac{|\delta \sigma_2|}{\sigma_2} \leq 0.15 \quad (38)$$

Estimations (38) show that maximal relative error in a determination of each residual stress component does not exceed 15 per cent. This is very good result in the course of implementing the hole drilling method for residual stress characterisation in graphite-epoxy laminated composite. But the value of the condition number (33)  $condA = 2.95$  demonstrates an excellent metrological capabilities of the approach developed. Thus, there is a hope that real error in residual stresses determination might be considerably low of estimations (38). A comparison of real interference fringe patterns and analogous artificial images presented in the following subsection contains the answer on this question.

## 6.2 Reference fringe patterns

The MSC/NASTRAN computer codes serves for numerical simulation essential for a visualisation of reference fringe patterns [16-18]. Plane shell elements of QUAD 4 type and generalised parameters (28) are used in the course of FEM calculations for specimen 1. Orthotropic square plate of  $80 \times 80 \times 6 \text{mm}^3$  with and without central through open hole of  $2r_0=2.5 \text{mm}$  diameter subjected to one-axis tension in each principal anisotropy direction is considered. Finite element mesh consists of about 20000 elements. Residual stress values along the hole edge obtained by FEM coincide with analogous data, which follow from formulae (8) and (9), within five per cent. A visualisation of reference fringe patterns is performed by using residual stress values from Table 1. Reference fringe patterns constructed for point 4, which correspond to real interferograms in Figure 5, are shown in Figure 9.

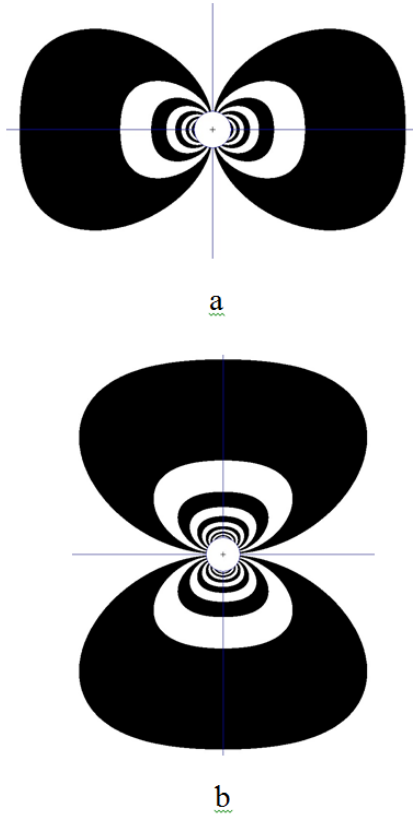


Fig. 9. Specimen 1. Reference fringe patterns visualised for point 4 in terms of in-plane displacement component  $u$  (a) and  $v$  (b).

A comparison of corresponding images in Figures 5a and 9a as well as in Figures 5b and 9b reveals some differences in the fringe patterns configuration. This circumstance might be attributed to the fact that numerical simulation implies generalized mechanical properties of layered composite material whereas real interferograms are referred to external face of the specimen. In any case this fact has to be taken into account if multiple-point over-deterministic approaches based on full-field displacement measurements are used for residual stress characterisation [10-14]. The method developed in this paper allows us effective accuracy analysis by comparing fringe order differences obtained experimentally in principal stress directions and the same data inherent in analogous artificial images. These parameters calculated accordingly relations (27) for point 4 from Table 1 are listed in Table 3. The values of  $u$ -displacement components obtained by both ways absolutely coincide. A

difference in  $v$ -displacement components consists of one fringe.

Table 3. Comparison of fringe orders differences and residual stress values corresponding to real interferograms and artificial interferometric images for specimen 1.

Fringe order differences in real interferograms		Values of real residual stress components	
$\Delta N_u^{Exp}$ , fringes	$\Delta N_v^{Exp}$ , fringes	$\sigma_1^{Exp}$ , MPa	$\sigma_2^{Exp}$ , MPa
10.0	13.0	73.4	61.4
Fringe order differences in reference fringe patterns		Values of conventional residual stress components	
$\Delta N_u^{Num}$ , fringes	$\Delta N_v^{Num}$ , fringes	$\sigma_1^{Num}$ , MPa	$\sigma_2^{Num}$ , MPa
10.0	12.0	72.0	57.9

Table 3 also includes the values of residual stress components, which are obtained by relations (25) from experimental and numerically simulated data. Relative errors in a determination of each residual stress component in the case involved can be estimated as:

$$|\delta\sigma_1| = \frac{|\sigma_1^{Exp} - \sigma_1^{Num}|}{\sigma_1^{Exp}} \leq 0.02, \quad (39)$$

$$|\delta\sigma_2| = \frac{|\sigma_2^{Exp} - \sigma_2^{Num}|}{\sigma_2^{Exp}} \leq 0.06$$

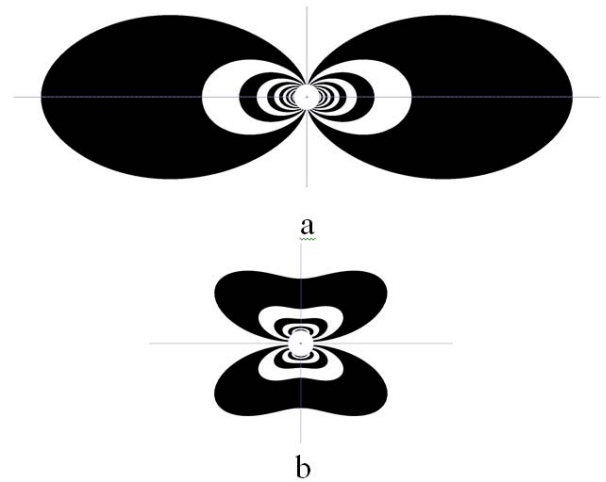


Fig. 10. Specimen 2. Reference fringe patterns visualised for point 5 in terms of in-plane displacement component  $u$  (a) and  $v$  (b).

A procedure of constructing reference fringe patterns is also performed for specimen 2 by using above-described numerical procedure and data (29). Artificial interferometric images visualised for point 5, which correspond to real interferograms in Figure 8, are shown in Figure 10. A comparison of corresponding images in Figures 8a and 10a as well as in Figures 8b and 10b again shows differences in the fringe patterns configuration. It should be noted that revealed differences are some more comparing with those obtained for specimen 1. But, comparing fringe order differences obtained experimentally in principal stress directions and the same data inherent in analogous artificial images demonstrates very good correlation. These parameters calculated accordingly relations (27) for points 2 and 5 from Table 2 are listed in Table 4. The values of  $u$ -displacement components obtained by both ways absolutely coincide. A difference in  $v$ -displacement components consists of half of the fringe.

Table 4. A comparison of fringe orders differences and residual stress values corresponding to real interferograms and artificial interferometric images for specimen 2.

Point number	Fringe order differences in real interferograms		Values of real residual stress components	
	$\Delta N_u^{Exp}$ , fringes	$\Delta N_v^{Exp}$ , fringes	$\sigma_1^{Exp}$ , MPa	$\sigma_2^{Exp}$ , MPa
2	9.5	6.0	81.0	46.0
5	12.0	7.5	81.0	46.0
Point number	Fringe order differences in reference fringe patterns		Values of conventional residual stress components	
	$\Delta N_u^{Num}$ , fringes	$\Delta N_v^{Num}$ , fringes	$\sigma_1^{Num}$ , MPa	$\sigma_2^{Num}$ , MPa
2	9.5	5.5	79.4	44.1
5	12.0	7.0	80.4	44.7

Relative errors in a determination of each residual stress component estimated accordingly inequalities (39) are:

$$\text{For point 2: } |\delta\sigma_1| \leq 0.02, |\delta\sigma_2| \leq 0.04. \quad (40)$$

$$\text{For point 5: } |\delta\sigma_1| \leq 0.007, |\delta\sigma_2| \leq 0.03. \quad (41)$$

Data of inequalities (39)-(41) are not bad comparing with errors obtained as the results of numerical experiments presented in work [13]. But we have to say that estimations (39)-(41) correspond to the real experiments.

An availability of the regular positively defined square [2x2] matrix **A** from direct equation (2) allows us an estimation of the upper bound of measurement accuracy in the explicit form. Refined estimations of real errors based on constructing reference fringe patterns prove that these error values do not exceed six per cent. This accuracy is reliably reached when fringe order differences are evaluated by the naked eye of the operator without any doubts because an error value  $\delta N=0.5$  fringe means a difference between neighbouring bright and dark fringes. Thus, developed experimental procedure based on a calculation of fringe order differences for two pairs of surface points needs no special equipment for automated displacement field acquisition.

## 7 Conclusions

Novel method for a determination of principal residual stress components in composite plates is developed and verified. It is based on through hole drilling and further measurements of hole diameter increments in principal stress directions by electronic speckle-pattern interferometry. Theoretical and metrological foundations of the approach follow from the analytical solution of S.G. Lekhnitsky, which describes a stress concentration along the edge of central open hole in rectangular orthotropic plate under tension in principal anisotropy directions. Formulae for deriving residual stress components from initial experimental data represent by itself unequivocally solution of the properly posed inverse problem. This means that there is no need to involve FEM calibration and multiple-point over-deterministic procedures to solve residual stress problem. A formulation of the experimental method does not depend on mechanical properties of the orthotropic material. The accuracy of residual stress determination within six per cent is reached. Presented approach can be easily formulated for any  $\varphi$  value, which describes an

**PAPER TITLE RESIDUAL STRESS CHARACTERIZATION  
IN ORTHOTROPIC PLATE BY COMBINING  
HOLE-DRILLING METHOD AND SPECKLE INTERFEROMETRY**

angle between principal residual stress directions and principal anisotropy axes, by using formula (9).

## References

- [1] Parlevliet PP, Bersee HEN, Beukers A. Residual stresses in thermoplastic composites—a study of the literature. Part I: Formation of residual stresses. *Composites Part A: Applied Science and Manufacturing*, Vol. 37, No. 11, pp 1847–1857, 2006.
- [2] Parlevliet PP, Bersee HEN, Beukers A. Residual stresses in thermoplastic composites—a study of the literature. Part III: Effects of thermal residual stresses. *Composites Part A: Applied Science and Manufacturing*, Vol. 38, No. 6, pp 1581–1596, 2007.
- [3] Stavrov D, Bersee NEN. Resistance welding of thermoplastic composites – an overview. *Composites Part A: Applied Science and Manufacturing*, Vol. 36, No. 1, pp 39–54, 2005.
- [4] Parlevliet PP, Bersee HEN, Beukers A. Residual stresses in thermoplastic composites—a study of the literature. Part II: Experimental techniques. *Composites Part A: Applied Science and Manufacturing*, Vol. 38, No. 3, pp 651–665, 2006.
- [5] Dubé M, Hubert P, Yousefpour A, Denault J. Resistance welding of thermoplastic composites skin/stringer joints. *Composites Part A: Applied Science and Manufacturing*, Vol. 38, No.12, pp 2541–2552, 2007.
- [6] Lu C, Chen P, Yu Q, Gao J, Yu B. Thermal Residual Stress Distribution in Carbon Fiber/Novel Thermal Plastic Composite. *Applied Composite Materials*, Vol. 15, No. 3, pp 157–169, 2008.
- [7] Schajer GS, Yang L. Residual-stress measurement in orthotropic materials using the hole-drilling method. *Experimental Mechanics*, Vol. 34, No. 4, pp 324–333, 1994.
- [8] Sicot O, Gong XL, Cherouat A, Lu J. Determination of residual stress in composite laminates using the incremental hole-drilling method. *Journal of Composite Materials*, Vol. 37, No. 9, pp 831-844, 2003.
- [9] Pagliaro P, Zuccarello B. Residual stress analysis of orthotropic materials by the through-hole drilling method. *Experimental Mechanics*, Vol.47, No.2, pp 217–236, 2007.
- [10] Cárdenas-García JF, Ekwaro-Osire S, Berg JM, Wilson WH. Non-linear least-square solution to the moiré hole method problem in orthotropic materials. Part I: residual stresses. *Experimental Mechanics*, Vol.45, No.4, pp 301–313, 2005.
- [11] Cárdenas-García JF, Ekwaro-Osire S, Berg JM, Wilson WH. Non-linear Least-squares Solution to the Moiré Hole Method Problem in Orthotropic Materials. Part II: Material Elastic Constants. *Mechanics*, Vol.45, No.4, pp 314–324, 2005.
- [12] Cárdenas-García JF, Preidikman S, Shabana YM. Solution of the moiré hole drilling method using a finite-element-method-based approach. *International Journal of Solids and Structures* Vol.46, No.22-23, pp 6751–6766, 2006.
- [13] Baldi A. Full field methods and residual stress analysis in orthotropic material. I Linear approach. *International Journal of Solids and Structures*, Vol.44, No.25-26, pp 8229–8243, 2007.
- [14] Baldi A. Full field methods and residual stress analysis in orthotropic material. II Nonlinear approach. *International Journal of Solids and Structures*, Vol.44, No.25-26, pp 8244–8258, 2007.
- [15] Lekhnitsky SG. *Theory of Elasticity of an Anisotropic Elastic Body*. Holden-day, Translation of 1950 Russian edition, 1963.
- [16] Pisarev VS, Balalov VV, Aistov VS, Bondarenko MM, Yustus MG. Reflection hologram interferometry combined with hole drilling techniques as an effective tool for residual stress field investigation in thin-walled structures. *Optics and Lasers in Engineering*, Vol.36, No.6, pp 551–597, 2001.
- [17] Pisarev VS, Bondarenko MM, Chernov AV, Vinogradova AN. General approach to residual stress determination in thin-walled structures by combining the hole drilling method and reflection hologram interferometry. *International Journal of Mechanical Sciences*, Vol.47, No.9, pp 1350–1376, 2005.
- [18] Pisarev VS, Odintsev IN, Apalkov AA, Chernov AV. Role of high-quality interference fringe patterns for the residual stress determination by the hole-drilling method. *Visualization of Mechanical Processes* Vol. 1, No. 1, DOI: 10.1615/VisMechProc.v1.i1.40, 2011.
- [19] Laermann KH. Reliable evaluation of measured data—an inverse problem. In: Juptner W, Osten W, Editors. Fringe 2001. Proc. of the 4th Int. *Workshop on Automatic Processing of Fringe Patterns*. Paris: Elsevier, 2001. p. 443-450.
- [20] Rastogi P. *Digital speckle pattern interferometry and related techniques*. Wiley, West Sussex: 2001.
- [21] Maclead N, Kapur DN. A kinematically designed mount for the precise location of specimen for holographic interferometry. *Journal of Physics E: Scientific Instruments*, Vol.6, pp 423-424, 1973.
- [22] Shchepinov VP, Pisarev VS. *Strain and Stress Analysis by Holographic and Speckle Interferometry*. Chichester: John Wiley, 1996.
- [23] Lankaster P. *Theory of matrices*. New York-London: Academic Press, 1969.
- [24] Forsythe GE, Malcolm MA, Moler CB. *Computer methods for mathematical computations*. Prentice-Hall, 1977.

## Copyright Statement

The authors confirm that they, and/or their company or organization, hold copyright on all of the original material included in this paper. The authors also confirm that they have obtained permission, from the copyright holder of any third party material included in this paper, to publish it as part of their paper. The authors confirm that they give permission, or have obtained permission from the copyright holder of this paper, for the publication and distribution of this paper as part of the ICAS 2014 proceedings or as individual off-prints from the proceedings.